



ELSEVIER

Computers and Chemical Engineering 26 (2002) 1153–1169

**Computers
& Chemical
Engineering**

www.elsevier.com/locate/comchemeng

Simulation, estimation and control of size distribution in aerosol processes with simultaneous reaction, nucleation, condensation and coagulation

Ashish Kalani, Panagiotis D. Christofides *

Department of Chemical Engineering, University of California, Los Angeles, 5531 Boetter Hall, 405 Hilgard Avenue, Box 951592, Los Angeles, CA 90095-1592, USA

Accepted 22 February 2002

Abstract

This article presents a comprehensive study on simulation, estimation and control of size distribution in aerosol processes with simultaneous chemical reaction, nucleation, condensation and coagulation. Initially, a typical aerosol process is considered and a detailed population balance model is presented which describes how the aerosol size distribution evolves with time. The population balance is complemented with mass and energy balances that describe the evolution of the continuous phase species and temperature of the system. Sectional representations and unimodal lognormal moment approximations of the population balance model are then derived and solved. It is found that the moment model provides reasonably accurate estimates of the average properties of the aerosol size distribution computed by the sectional model for long times. Then, a nonlinear state estimator is constructed on the basis of the moment model, which employs measurements of the geometric average particle diameter to compute the evolution of the average properties of the aerosol size distribution. Finally, a nonlinear controller is designed on the basis of the moment model and is implemented on the sectional model to achieve an aerosol size distribution with desired geometric average particle diameter. The robustness properties of the nonlinear estimator and controller with respect to significant parametric model uncertainty are successfully tested through computer simulations. © 2002 Elsevier Science Ltd. All rights reserved.

Keywords: Particle size distribution; Aerosol processes; Nonlinear state estimation; Nonlinear control

1. Introduction

Aerosol processes are commonly used for the large scale production of nano and micron sized particles from direct gas phase chemical reaction. Aerosol products, such as TiO_2 and B_4C , find widespread industrial use as pigments, reinforcing agents, ceramic powders, carbon blacks and semiconductor materials. The growth process of aerosol particles may be divided into different stages. The first stage is gas phase chemical reaction, which produces monomers or molecules of the condensable species (Friedlander, 1977, 1983). In the next stage, these monomers coalesce to form unstable

clusters, which grow further by monomer condensation. The clusters nucleate into stable aerosol particles, once a thermodynamic critical cluster size is attained. Growth then occurs mainly by coagulation and condensation; the relative strength of each greatly affects the particle size and morphology. It is now well-understood that the physico-chemical and mechanical properties of materials made with participates depend heavily on the characteristics of the corresponding particle size distribution (PSD; for example, a nearly monodisperse PSD is required for titania pigments to obtain the maximum hiding powder per unit mass). Therefore, the problem of synthesizing and implementing high-performance model-based feedback control systems on particulate processes to achieve PSDs with desired characteristics has significant industrial value.

Aerosol processes are modeled by population balance equations, which give rise to nonlinear partial integro-

* Corresponding author. Tel.: +1-310-794-1015; fax: +1-310-206-4107

E-mail address: pdc@seas.ucla.edu (P.D. Christofides).

differential equation systems (where the independent variables are time and one or more internal particle coordinates, such as particle volume and shape). The nonlinearities usually arise from complex reaction, nucleation, condensation and coagulation rates and their nonlinear dependence on temperature. A variety of solution techniques have been developed to address the complexity at various levels. Under appropriate simplifying assumptions, analytical solutions have been developed to solve the population balance equation (such as the use of Laplace transforms for solving agglomeration problems in the absence of particle growth Friedlander, 1977); however, in most cases, one needs to resort to numerical solutions. One of the standard numerical techniques is to discretize the population balance equation using finite difference/element methods (see, for example, Hounslow, 1990; Hill & Ng, 1995, 1996; Kumar & Ramkrishna, 1996a,b; Nicmanis & Hounslow, 1998; Mantzaris, Daoutidis & Srienc, 2001 and the review paper Ramkrishna, 1985), but these methods suffer from extremely large computational requirements which cannot be accommodated by conventional computers. Sectional models offer a computationally less demanding solution by approximating the continuous size distribution by a finite number of sections within which the PSD function is assumed to be constant (Gelbart & Seinfeld, 1978; Gelbard, Tambour & Seinfeld, 1980; Landgrebe & Pratsinis, 1990). But even these models are unsuitable for the synthesis of practically-implementable feedback controllers. Fortunately, in most cases, the aerosol size distribution can be adequately described by lognormal functions; this makes it possible to develop moment models which describe the evolution of the key moments of the system as well as important bulk properties, such as the geometric average volume of the size distribution. Moment models have proven to be simpler to analyze and simulate (e.g. Frenklach & Harris, 1987; Pratsinis, 1988). An alternative approach to population balance modeling involves the use of Monte Carlo techniques (Akhtar, Lipscomb & Pratsinis, 1994; Van Peborgh Gooch & Hounslow, 1996; Tandon & Rosner, 1999).

In spite of the rich literature on population balance modeling, numerical solution and dynamical analysis of aerosol processes, the issue of population balance model-based feedback control of size distribution in aerosol processes has received little attention in the past. Even the broader subject of control of systems modeled by population balance equations has been inadequately explored. Prior research in this area has primarily focused on understanding the observability and controllability properties of population balance equations (Hashemi & Epstein, 1982; Semino & Ray, 1995a), stability analysis using Laplace transform and Lyapunov functional (e.g. Hale & Verduyn Lunel, 1993; Rawlings & Ray, 1987) and the application of

conventional control schemes (e.g. proportional-integral, proportional-integral-derivative, self-tuning control) to crystallizers and emulsion polymerization processes (e.g. Semino & Ray, 1995b; Rohani & Bourne, 1990; Dimitratos, Elicabe & Georgakis, 1994). Unfortunately, conventional control schemes perform poorly in the face of severe process nonlinearities, and may even lead to destabilization of the closed loop system. These limitations of conventional control schemes, together with recent developments in measurement technology based on laser diffraction techniques which allow nonintrusive and fast on-line measurement of key properties of PSDs at very high frequency (see, for example, Rawlings, Miller & Witkowski, 1993 for an excellent review of the available measurement technology), have motivated research efforts towards synthesizing for nonlinear model-based feedback controllers on spatially-homogeneous particulate processes (Eaton & Rawlings, 1990; Chiu & Christofides, 1999, 2000; El-Farra, Chiu & Christofides, 2001) with application to size distribution control in batch (Eaton & Rawlings, 1990) and continuous crystallizers (Chiu & Christofides, 1999, 2000; El-Farra et al., 2001).

Recently, motivated by the development of fast on-line measurement techniques and the availability of high-performance software and hardware which allows instantaneous calculation of the appropriate control actions on the basis of advanced model-based control algorithms, we initiated an effort to develop measurement/model-based control strategies for precise control of size distribution in aerosol processes. Even though aerosol systems are characterized by very small residence times, design and implementation of advanced feedback control techniques could make a significant impact on the industrial practice of aerosol processing by reducing product variability and off-spec aerosol production. More specifically, our research work focused on moment-model based control of a class of spatially-inhomogeneous aerosol processes with application to a titania aerosol reactor (Kalani & Christofides, 1999, 2000). However, in these studies, the developed nonlinear controllers were implemented on moment model approximations of the population balances, and therefore, the important issue of evaluating the controller performance on the basis of accurate discretizations of the population balance (for example, sectional approximations) was not studied. Motivated by this, the objective of this article is to present a comprehensive study of simulation, estimation and control of size distribution in an aerosol process with simultaneous chemical reaction, nucleation, condensation and coagulation using detailed sectional discretizations of the population balance. We choose to focus on an aerosol system that involves all the above mentioned phenomena rather than a specific aerosol process

(where some of these mechanisms may not be important; see Kalani & Christofides, 2000 for example) because our objective is to present and evaluate general simulation, estimation and feedback control techniques that are applicable to a broad range of aerosol systems.

The manuscript is structured as follows: Initially, a general aerosol population balance model is presented which accounts for simultaneous chemical reaction, nucleation, condensation and coagulation and describes how the aerosol size distribution evolves with time. The population balance is complemented with mass and energy balances that describe the evolution of the continuous phase species and temperature of the system. Sectional representations and lognormal moment approximations of the population balance model are then derived and solved. It is found that the moment model provides reasonably accurate estimates of the average properties of the aerosol size distribution computed by the sectional model for long times. Then, a nonlinear state estimator is constructed on the basis of the moment model, which employs measurements of the geometric average particle diameter to compute the evolution of the average properties of the aerosol size distribution. Finally, a nonlinear controller is designed on the basis of the moment model and is implemented on the sectional model to achieve an aerosol size distribution with desired geometric average particle diameter. The robustness properties of the nonlinear estimator and controller with respect to significant parametric model uncertainty are successfully tested through computer simulations.

2. Preliminaries

2.1. Spatially-homogeneous aerosol process model

We consider general aerosol processes with simultaneous chemical reaction, nucleation, condensation and coagulation. A general mathematical model which describes the temporal evolution of the PSD in such aerosol processes can be obtained from a population balance and consists of the following nonlinear partial integro-differential equation (Friedlander, 1977):

$$\begin{aligned} \frac{\partial n}{\partial t} + \frac{\partial(G(\bar{x}, v)n)}{\partial v} - I(v^*)\delta(v - v^*) \\ = \frac{1}{2} \int_0^v \beta(v - \bar{v}, \bar{v}, \bar{x})n(v - \bar{v}, t)n(\bar{v}, t)d\bar{v} \\ - n(v, t) \int_0^\infty \beta(v, \bar{v}, \bar{x})n(\bar{v}, t)d\bar{v} \end{aligned} \quad (1)$$

where $n(v, t)$ denotes the PSD function, v is the particle volume, t is the time, $G(\bar{x}, v)$, $I(v^*)$, $\beta(v - \bar{v}, \bar{v}, \bar{x})$ are nonlinear scalar functions and $\delta(\cdot)$ is the standard Dirac function.

On the other hand, a mathematical model which predicts the temporal evolution of the concentrations of species and temperature of the gas phase can be obtained from mass and energy balances and has the following form:

$$\frac{d\bar{x}}{dt} = \bar{f}(\bar{x}) + \bar{g}(\bar{x})u(t) + \bar{A} \int_0^\infty a(\eta, v, \bar{x})dv \quad (2)$$

where $\bar{x}(t)$ is an n -dimensional vector of state variables that depend on time, \bar{A} is constant matrix, $\bar{f}(\bar{x})$, $\bar{g}(\bar{x})$, $a(\eta, v, \bar{x})$ are nonlinear vector functions and $u(t)$ is the time-varying manipulated input (e.g. wall temperature). The term $\bar{A} \int_0^\infty a(\eta, v, \bar{x})dv$ accounts for mass and heat transfer from the continuous phase to all the particles in the population.

In the population balance of Eq. (1), the term $\partial n / \partial t$ describes the rate of change of particle concentration in the particle volume interval $v, v + dv$. The terms $\partial(G(\bar{x}, v)n) / \partial v$ and $I(v^*)\delta(v - v^*)$ account for the loss or gain of particles by condensation at rate G and the formation of new particles of critical volume v^* by nucleation at rate I , respectively. Finally, the gain and loss of particles by Brownian coagulation is described by the terms:

$$\begin{aligned} \frac{1}{2} \int_0^v \beta(v - \bar{v}, \bar{v}, \bar{x})n(v - \bar{v}, t)d\bar{v}, \quad \text{and} \\ n(v, t) \int_0^\infty \beta(v, \bar{v}, \bar{x})n(\bar{v}, t)d\bar{v}, \end{aligned} \quad (3)$$

respectively. $G(\bar{x}, v)$ and $\beta(\bar{x}, v_1, v_2)$ are the diffusional condensation growth function and the Brownian coagulation coefficient, respectively, for which two different expressions are used for the free molecule size and continuum size regimes (Pratsinis, 1988): (a) for the free molecule size regime:

$$\begin{aligned} G_{FM}(\bar{x}, v) = B_1 v^{1/3}(S - 1), \quad B_1 = (36\pi)^{1/3} v_0 n_s \left(\frac{k_B T}{2\pi m_0} \right)^{1/2} \\ \beta_{FM}(\bar{x}, v_1, v_2) = B_2 \left(\frac{1}{v_1} + \frac{1}{v_2} \right)^{1/2} (v_1^{1/3} + v_2^{1/3})^2, \\ B_2 = \left(\frac{3}{4} \pi \right)^{1/3} \left(\frac{6k_B T v_0}{m_0} \right)^{1/2}, \end{aligned} \quad (4)$$

and (b) for the continuum size regime:

$$\begin{aligned} G_C(\bar{x}, v) = B_3 v^{1/3}(S - 1), \quad B_3 = (48\pi^2)^{1/3} D_f v_0 n_s, \quad D_f \\ = \lambda \frac{(8k_B T / \pi m_0)^{1/2}}{3} \\ \beta_C(\bar{x}, v_1, v_2) = B_4 \left(\frac{C(v_1)}{v_1^{1/3}} + \frac{C(v_2)}{v_2^{1/3}} \right) (v_1^{1/3} + v_2^{1/3}), \\ B_4 = \frac{2k_B T}{3\mu} \end{aligned} \quad (5)$$

In Eqs. (4) and (5), S is the saturation ratio, T is the temperature, D_f is the condensable vapor diffusivity, λ

is the mean free path of the gas ($\lambda = \nu\pi M_w/2k_B T N_{av}$, where ν and M_w are the kinematic viscosity and molecular weight of the fluid, respectively, and N_{av} is the Avogadro's number), μ is the viscosity of the fluid, n_s is the monomer concentration at saturation ($n_s = P_s/k_B T$, where P_s is the saturation pressure), m_0 is the monomer mass, v_0 is the monomer volume, r is the particle radius, $C(v) = 1 + B_5\lambda/r$ is the Cunningham correction factor and $B_5 = 1.257$. Expressions for the diffusional condensation growth function and the Brownian coagulation coefficient for the entire particle size spectrum are based on the work of Fuchs and Sutugin (see, for example, Friedlander, 1977; Xiong & Pratsinis, 1991) and have the following form:

$$G(\bar{x}, v) = (48\pi^2)^{1/3} D_{\bar{x}} n_s v_0 (S - 1) \times v^{1/3} \left(\frac{1 + Kn}{1 + 1.71Kn + 1.333Kn^2} \right) \quad (6)$$

$$\beta(\bar{x}, v_1, v_2) = 2\pi(L_{r1} + L_{r2})(d_{p1} + d_{p2}) \times \left[\frac{d_{p1} + d_{p2}}{d_{p1} + d_{p2} + 2g_{12}} + \frac{8(L_{r1} + L_{r2})}{\bar{c}_{12}(d_{p1} + d_{p2})} \right]^{-1}$$

$$L_{ri} = \frac{k_B T}{3\pi\mu d_{pi}} \left[\frac{5 + 4Kn_i + 6Kn_i^2 + 18Kn_i^3}{5 - Kn_i + (8 + \pi)Kn_i^2} \right]$$

$$g_{12} = (g_1^2 + g_2^2)^{1/2}$$

$$g_i = (3d_{pi}l_i)^{-1} [(d_{pi} + l_i)^3 - (d_{pi}^2 + l_i^2)^{3/2}] - d_{pi}$$

$$l_i = \frac{8L_{ri}}{\pi c_i}$$

$$c_i = \left(\frac{8k_B T}{\pi m_i} \right)^{1/2}$$

$$c_{12} = (c_1^2 + c_2^2)^{1/2} \quad (7)$$

where d_{pi} , m_i and K_{ni} are the diameter, mass and Knudsen number ($K_{ni} = 2\lambda/d_{pi}$), respectively, for one of the colliding particles with volume v_i . Finally, the nucleation rate $I(v^*)$ is assumed to follow the classical Becker–Doring theory and is given by the following expression (Pratsinis, 1988):

$$I = n_4^2 s_0 \left(\frac{k_B T}{2\pi m_0} \right)^{1/2} S^2 \left(\frac{2}{9\pi} \right)^{1/3} \sum^{1/2} \exp\left(-k^* \ln \frac{S}{2} \right) \quad (8)$$

where s_0 is the monomer surface area and k^* is the number of monomers in the critical size nucleus which is given by:

$$k^* = \frac{\pi}{6} \left(\frac{4\Sigma}{\ln S} \right)^3 \quad (9)$$

where $\Sigma = \gamma v_0^{2/3}/k_B T$ and γ is the surface tension.

Remark 1: Referring to the system of Eqs. (1) and (2), several remarks are in order (a) the manipulated input

$u(t)$, enters the system through Eq. (2) (mass and energy balance model); this assumption is usually satisfied in most practical applications where the wall temperature is chosen as the manipulated input; (b) the nonlinearities in Eq. (2) appear in an additive fashion (e.g. complex reaction rates, Arrhenius dependence of reaction rates on temperature); and (c) the effect of particle curvature on aerosol evaporation rate (Kelvin effect) is neglected; this is done to simplify the form of the right hand side of the moment model through direct expression of various integral terms over the entire particle size spectrum in terms of the moments of the aerosol size distribution (see Section 4).

Remark 2: In Eq. (4), the expansion of the expression for β_{FM} yields an unmanageable number of terms necessary for covering a wide range of the particle sizes. To simplify calculations in future sections, the following approximation will be made:

$$\left(\frac{1}{v} + \frac{1}{\bar{v}} \right)^{1/2} = b \left(\frac{1}{v^{1/2}} + \frac{1}{\bar{v}^{1/2}} \right) \quad (10)$$

Coefficient b depends on the geometric standard deviation and moments of the PSD (Lee, Chen & Gieseke, 1984).

3. Sectional model

Sectional models divide the continuous PSD into a finite number of sections within which the size distribution function is assumed to be constant. A single conservation equation is developed for a given integral property in each section. This limits the number of conservation equations that need to be solved for generating the size distribution, to the number of sections being considered. The accuracy and computational speed of sectional models depends on the number of sections employed, on the selection of the numerically conserved integral property of the distribution, and on the treatment of the lower end of the size distribution (Gelbard et al., 1980; Landgrebe & Pratsinis, 1990).

3.1. Theoretical development

We assume that the entire particle volume spectrum is divided into m arbitrary sections, and consider a general property, $q(v, t)$, of the aerosol size distribution having the following form (Gelbard et al., 1980):

$$q(v, t) = \alpha v^\gamma n(v, t) \quad (11)$$

where α and γ are constants. An integral quantity of the aerosol property in a given section I , may then be defined as:

$$Q_l(t) = \int_{v_{l-1}}^{v_l} q(v, t) dv_l \quad l = 1, 2, \dots, m \quad (12)$$

where v_{l-1} and v_l denote the volumes of the smallest and largest particles, respectively, in section l (note that v_0 denotes the volume of the monomer). To obtain a closed set of equations for the sectional model, it is assumed that the property $q(v, t)$ is constant within a given section l , i.e. $q(v, t) = q_l(t)$, where $q_l(t)$ is a constant for section l . Substituting from Eqs. (11) and (12), we thus obtain an equation relating the size distribution function $n(v, t)$ to the corresponding integral sectional property $Q_l(t)$:

$${}^2\bar{\beta}_{i,l} = \int_{x_{i-1}}^{x_i} \int_{x_{l-1}}^{x_l} \frac{[\theta(u+v > x_l)u^\gamma - \theta(u+v < x_l)((u+v)^\gamma - u^\gamma)]\beta(u, v)}{\alpha u^\gamma v^\gamma (x_i - x_{i-1})(x_l - x_{l-1})} dudv \quad 2 \leq l \leq m, \quad i < l \quad (16)$$

$${}^3\bar{\beta}_{l,l} = \int_{x_{l-1}}^{x_l} \int_{x_{l-1}}^{x_l} \frac{[\theta(u+v > x_l)(u^\gamma + v^\gamma) + \theta(u+v < x_l)[(u^\gamma + v^\gamma) - (u+v)^\gamma]]\beta(u, v)}{\alpha u^\gamma v^\gamma (x_l - x_{l-1})^2} dv du \quad 1 \leq l \leq m \quad (17)$$

$${}^4\bar{\beta}_{i,l} = \int_{x_{i-1}}^{x_i} \int_{x_{l-1}}^{x_l} \frac{u^\gamma \beta(u, v)}{\alpha u^\gamma v^\gamma (x_i - x_{i-1})(x_l - x_{l-1})} dudv \quad 1 \leq l \leq m, \quad i > l \quad (18)$$

$$n(v, t) = \frac{Q_l(t)}{\alpha v^\gamma (v_l - v_{l-1})} \quad (13)$$

Following the derivation described in Appendix A, we obtain the following integro-differential equation representing the rate of change of $Q_l(t)$ in section l :

$$\begin{aligned} \frac{dQ_l}{dt} = & \alpha v^* I(v^*) \theta(v_{l-1} < v^* < v_l) + \frac{1}{2} \sum_{i=1}^{l-1} \sum_{j=1}^{l-1} {}^1\bar{\beta}_{i,j,l} Q_i Q_j \\ & - Q_l \sum_{i=1}^{l-1} {}^2\bar{\beta}_{i,l} Q_i - \frac{1}{2} {}^3\bar{\beta}_{l,l} Q_l^2 - Q_l \sum_{i=l+1}^m {}^4\bar{\beta}_{i,l} Q_i \\ & + \xi_{l-1} Q_{l-1} - \xi_l Q_l \end{aligned} \quad (14)$$

The first term on the right-hand side of Eq. (14) represents the increase in Q_l due to nucleation of new particles in section l (the expression, $\theta(\text{condition})$ equates to 1 if the condition is satisfied or 0 if it is not). The second and third terms (both evaluated only for $l > 1$) represent the increase in Q_l due to coagulation in the lower sections, and due to the coagulation phenomena between particles in the lower sections and those in section l , respectively. The next two terms (the second of these two terms is evaluated only for $l < m$) give the decrease in Q_l due to loss of particles to the higher sections by coagulation in section l , and due to coagulation of particles in section l , with those in higher sections, respectively. The last two terms represent the net change in Q_l due to an influx of particles growing due to the condensation of monomers, from section $l-1$, and the outflux of particles to section $l+1$ due to

condensation (the first of these two terms is evaluated only for $l > 1$, and the second is evaluated only for $l < m$). The collision integrals $\beta_{x,y,z}$ have the following form:

$$\begin{aligned} & {}^1\bar{\beta}_{i,j,l} \\ & = \int_{x_{i-1}}^{x_i} \int_{x_{j-1}}^{x_j} \frac{\theta(x_{l-1} < u+v < x_l)(u+v)^\gamma \beta(u, v)}{\alpha u^\gamma v^\gamma (x_i - x_{i-1})(x_j - x_{j-1})} dudv \\ & \quad 2 \leq l \leq m, \quad 1 \leq i, j \leq l \end{aligned} \quad (15)$$

The variable ξ_l has the following form (Friedlander, 1977):

$$\xi_l = \frac{\omega v_l^{1/2}}{\Delta v_l} \left(\frac{1 + Kn_l}{1 + 1.71Kn_l + 1.333kn_l^2} \right) \quad (19)$$

where $w = (48\pi^2)^{1/3} D_f n_s v_0 (S-1)$, D_f is the diffusion coefficient of the condensing species, and $\Delta v_l = v_l - v_{l-1}$. A monomer balance for the system gives the following equation for the rate of change of the monomer concentration n_1 :

$$\begin{aligned} \frac{dn_1}{dt} = & R_r N_{av} - Ik^* - \omega \sum_{l=1}^m \frac{Q_l}{\alpha v^\gamma (v_l - v_{l-1})} \int_{v_{l-1}}^{v_l} v^{1/3} \\ & \frac{1 + Kn}{1 + 1.71Kn + 1.333Kn^2} dv \end{aligned} \quad (20)$$

where R_r is the chemical reaction rate.

4. Lognormal aerosol moment model

4.1. Moment model

Even though sectional models put a limit on the number of equations required to approximately solve the population balance model, the computational requirements of the solution method make them unsuitable for use in systems that generate responses in real time. Moment models provide adequate simplification by modeling the key average bulk properties of the evolving product, which may then be used to generate

the approximate PSD under the assumption of a self-preserving form (Williams & Loyalka, 1991). For the purpose of this study, the k th moment is defined as the particle volume weighted summation of the particle number density function:

$$M_k(t) = \int_0^\infty v^k n(v, t) dv, \quad (21)$$

In this subsection, the ODEs describing the temporal evolution of the three leading moments (i.e. the zeroth, first and second moments) of the size distribution for the free molecule size, continuum size regimes, are presented. The derivation of these equations from the population balance equation is given in Appendix B.

4.1.1. Free molecule size regime

The temporal evolution of the zeroth moment M_0 (particle concentration), which is affected by nucleation and coagulation, is given by:

$$\frac{dM_0}{dt} = I - b_0 B_2 (M_{2/3} M_{-1/2} + 2M_{1/3} M_{-1/6} + M_{1/6} M_0) \quad (22)$$

where the coefficient b_0 is used as b in Eq. (10) and is calculated for the zeroth moment. The evolution of M_1 (aerosol volume), which is affected by nucleation and condensation, is given by:

$$\frac{dM_1}{dt} = Iv^* + B_1(S-1)M_{2/3} \quad (23)$$

Finally, the second moment, M_2 , depends on nucleation, condensation and coagulation and is described by:

$$\frac{dM_2}{dt} = Iv^{*2} + 2B_1(S-1)M_{5/3} + 2b_2 B_2 (M_{5/3} M_{1/2} + 2M_{4/3} M_{5/6} + M_{7/6} M_1) \quad (24)$$

where b_2 is used as b_0 but for the coagulation kernel of the second moment.

Table 1
Dimensionless variables for the model of Eqs. (31)–(36)

$N = M_0/n_s$	Aerosol concentration
$V = M_1/n_s v_0$	Aerosol volume
$V_2 = M_2/n_s v_0^2$	Second aerosol moment
$\tau = (2\pi m_0/k_B T)^{1/2} / n_s S_0$	Characteristic time for particle growth
$K = (2k_B T/3\mu)n_s \tau$	Coagulation coefficient
$K_{n_0} = \lambda/r_0$	Monomer Knudsen number
$I' = I/(n_s/\tau)$	Nucleation rate
$R'_\tau = R_\tau/(n_s/\tau)$	Reaction rate group
$v'_g = v_g/v_0$	
$r'_g = r_g/r_0$	
$\theta = t/\tau$	

4.1.2. Continuum size regime

Similar to the case of the free molecule regime, the dynamics of the zeroth and second moments of the aerosol size distribution in the continuum size regime is described by the following ODE system:

$$\frac{dM_0}{dt} = I - B_4$$

$$[M_0^2 + M_{1/3} M_{-1/3} + B_5 \lambda \left(\frac{4\pi}{3}\right)^{1/5} (M_0 M_{-1/3} + M_{1/3} M_{-2/3})], \quad (25)$$

$$\frac{dM_1}{dt} = Iv^* + B_3(S-1)M_{1/3}, \quad (26)$$

$$\frac{dM_2}{dt} = Iv^{*2} + 2B_3(S-1)M_{4/3} + 2B_4$$

$$[M_1^2 + M_{4/3} M_{2/3} + B_5 \lambda \left(\frac{4\pi}{3}\right)^{1/3} (M_1 M_{2/3} + M_{1/3} M_{4/3})] \quad (27)$$

4.2. Lognormal particle size distribution

Studies suggest that aerosol PSDs can be adequately described by unimodal lognormal functions. This result makes it possible to develop a moment model for the aerosol process in terms of the three leading moments of the size distribution. The lognormal distribution is given (Xiong & Pratsinis, 1991) as:

$$n(v) = \frac{1}{3\sqrt{2\pi} \ln \sigma} \exp\left(-\frac{\ln^2(v/v_g)}{18 \ln^2 \sigma}\right) \frac{1}{v} \quad (28)$$

where v_g is the geometric average particle volume and σ is the standard deviation. v_g and σ may be expressed in terms of the first three moments of the distribution according to the following relations (Brock, Kuhn & Zehavi, 1986):

$$v_g = \frac{M_1^2}{M_0^{3/2} M_2^{1/2}}, \quad \ln^2 \sigma = \frac{1}{9} \ln\left(\frac{M_0 M_2}{M_1^2}\right). \quad (29)$$

Further, the moment description of the system may be closed as follows:

$$M_k = M_0 v_g^k \exp\left(\frac{9}{2} k^2 \ln^2 \sigma\right) \quad (30)$$

Clearly, the three leading moments are sufficient to generate the lognormal PSD. By expressing the other moments in Eqs. (22)–(27) in terms of the zeroth, first and second moments through the use of Eqs. (29) and (30), a set of moment equations representing the dynamics of the leading moments may be obtained. The zeroth and second moment equations for the free molecule size and continuum size regimes may be combined to describe the aerosol dynamics over the entire particle size spectrum by using the

harmonic average of the dimensionless coagulation rates in the free molecule size and continuum size regimes (the dimensionless harmonic average coagulation rate reduces to the appropriate limits in the two limiting size regimes and closely approximates the Fuchs-Sutugin approximation in the transition regime Pratsinis, 1988). This leads to the following equations (see Table 1 for the list of dimensionless variables):

Zeroth moment (aerosol concentration):

$$\frac{dN}{d\theta} = I' - \zeta N^2 \quad (31)$$

where:

$$\begin{aligned} \frac{1}{\zeta} &= \frac{1}{\zeta_{FM}} + \frac{1}{\zeta_C}, \quad \zeta_{FM} = r_g^{4/2} b_0 \\ &\left[\exp\left(\frac{25}{8} \ln^2 \sigma\right) + 2 \exp\left(\frac{5}{8} \ln^2 \sigma\right) + \exp\left(\frac{1}{8} \ln^2 \sigma\right) \right], \\ \zeta_C &= K \left[1 + \exp(\ln^2 \sigma) \right. \\ &\quad \left. + B_5 \left(\frac{K_{n_0}}{r'_g} \right) \exp\left(\frac{1}{2} \ln^2 \sigma\right) (1 + \exp(2 \ln^2 \sigma)) \right] \quad (32) \end{aligned}$$

First moment (aerosol volume):

$$\frac{dV}{d\theta} = I'k^* + \eta(S - 1)N \quad (33)$$

where:

$$\begin{aligned} \frac{1}{\eta} &= \frac{1}{\eta_{FM}} + \frac{1}{\eta_C}, \\ \eta_{FM} &= v_g^{2/3} \exp(2 \ln^2 \sigma), \quad \eta_C = \frac{4K_{n_0}}{3} v_g^{4/3} \exp\left(\frac{1}{2} \ln^2 \sigma\right) \quad (34) \end{aligned}$$

Second, aerosol moment:

$$\frac{dV_2}{d\theta} = I'k^{*2} + 2\varepsilon(S - 1)V + 2\zeta V^2 \quad (35)$$

where:

$$\begin{aligned} \frac{1}{\varepsilon} &= \frac{1}{\varepsilon_{FM}} + \frac{1}{\varepsilon_C}, \quad \frac{1}{\zeta} = \frac{1}{\zeta_{FM}} + \frac{1}{\zeta_C}, \\ \varepsilon_{FM} &= v_g^{4/2} b_2 \exp(8 \ln^2 \sigma), \\ \varepsilon_C &= \frac{4K_{n_0}}{3} v_g^{4/3} \exp\left(\frac{7}{2} \ln^2 \sigma\right), \\ \zeta_{FM} &= r_g^{4/2} b_2 \exp\left(\frac{3}{2} \ln^2 \sigma\right) \\ &\quad \times \left[\exp\left(\frac{25}{8} \ln^2 \sigma\right) + 2 \exp\left(\frac{5}{8} \ln^2 \sigma\right) \right. \\ &\quad \left. + \exp\left(\frac{1}{8} \ln^2 \sigma\right) \right], \zeta_C = K \left[1 + \exp \right. \end{aligned}$$

$$\begin{aligned} &(\ln^2 \sigma) + B_5 \left(\frac{K_{n_1}}{r'_g} \right) \exp\left(-\frac{1}{2} \ln^2 \sigma\right) \\ &\quad \left. \times (1 + \exp(-2 \ln^2 \sigma)) \right] \quad (36) \end{aligned}$$

Remark 3: In Eqs. (32) and (36), $b_0 = 0.633 + 0.0920\sigma^2 - 0.022\sigma^3$ and $b_2 = 0.39 + 0.5\sigma - 0.214\sigma^2 + 0.029\sigma^3$, respectively. These polynomial expressions are obtained as functions of σ by regression (Pratsinis, 1988).

Remark 4: The rate of change of S can be obtained from a monomer balance and is given by:

$$\frac{dS}{d\theta} = R'_r N_{av} - I'k^* - \eta(S - 1)N \quad (37)$$

5. Open-loop simulation study

In this section, we study and compare the results obtained from the simulation of the sectional and moment models for a typical aerosol process in a cylindrical volume with diameter D_T , and with the following chemical reaction: $A + B \rightarrow C$ and the following reaction rate: $R_r = k_r C_1 C_2$. Referring to the sectional model; by assuming the integral property Q_l in section l to be the number concentration N_l in the section (note that $\alpha = 1$ and $\gamma = 0$ in Eq. (11)), Eqs. (2), (14) and (20) produce the following mathematical model that describes the evolution of the number concentrations in the first m sections, together with that of the monomer and reactant concentrations and the fluid temperature:

$$\begin{aligned} \frac{dN_1}{dt} &= I(v^*)\theta(v_0 < v^* < v_1) - \frac{1}{2} {}^3\bar{\beta}_{1,1} N_1^2 - N_1 \sum_{i=2}^m {}^4\bar{\beta}_{i,1} N_i \\ &\quad - \zeta_1 N_1, \\ \frac{dN_l}{dt} &= I(v^*)\theta(v_{l-1} < v^* < v_l) + \frac{1}{2} \sum_{i=1}^{l-1} \sum_{j=1}^{l-1} {}^1\bar{\beta}_{i,j} N_i N_j \\ &\quad - N_l \sum_{i=1}^{l-1} {}^2\bar{\beta}_{i,l} N_i - \frac{1}{2} {}^3\bar{\beta}_{l,l} N_l^2 - N_l \sum_{i=l+1}^m {}^4\bar{\beta}_{i,l} N_i \\ &\quad + \zeta_{l-1} N_{l-1} - \zeta_l N_l, \quad 2 \leq l \leq m \\ \frac{dN_m}{dt} &= I(v^*)\theta(v_{m-1} < v^* < v_m) + \frac{1}{2} \sum_{i=1}^{m-1} \sum_{j=1}^{m-1} {}^1\bar{\beta}_{i,j} N_i N_j \\ &\quad - N_m \sum_{i=1}^{m-1} {}^2\bar{\beta}_{i,m} N_i - \frac{1}{2} {}^3\bar{\beta}_{m,m} N_m^2 + \zeta_{m-1} N_{m-1} \\ \frac{dn_0}{dt} &= k_r C_1 C_2 N_{av} - I'k^* - \omega \sum_{l=1}^m \frac{N_l}{(v_l - v_{l-1})} \int_{v_{l-1}}^{v_l} v^{1/3} \end{aligned}$$

Table 2
Process model parameters for the simulation study

$D_T = 0.05$ m	Process diameter
$P_0 = 1$ atm	Process pressure
$T_0 = 298$ K	Initial temperature
$Y_{10} = Y_{20} = 40$ ppm	Initial mole fraction of reactants
$U = 10.4$ J m ⁻² s ⁻¹ K ⁻¹	Overall coefficient of heat transfer
$\Delta H_r = 175.7$ K J ml ⁻¹	Heat of reaction
$C_p = 29.1$ J mol ⁻¹ K ⁻¹	Heat capacity of process fluid
$M_w = 14.0 \times 10^{-3}$ kg mol ⁻¹	Molecular weight of process fluid
$k = 11.4$ m ³ mol ⁻¹ s ⁻¹	Reaction constant
$\mu = 3.5 \times 10^{-6}$ kg m ⁻¹ s ⁻¹	Viscosity of process fluid
$\log P_s(\text{mmHg}) = -4644/T + 0.906$ $\log T - 0.00162T + 9.004$	Vapor pressure-temperature relation
$\gamma = 0.08$ Nm ⁻¹	Surface tension
$v_0 = 5.33 \times 10^{-29}$ m ³	Monomer volume
$R = 8.314$ J mol ⁻¹ K ⁻¹	Universal gas constant
$N_{av} = 6.023 \times 10^{23}$ # mol ⁻¹	Avogadro's constant
$k_B = 1.38 \times 10^{-23}$ J K ⁻¹	Boltzmann's constant

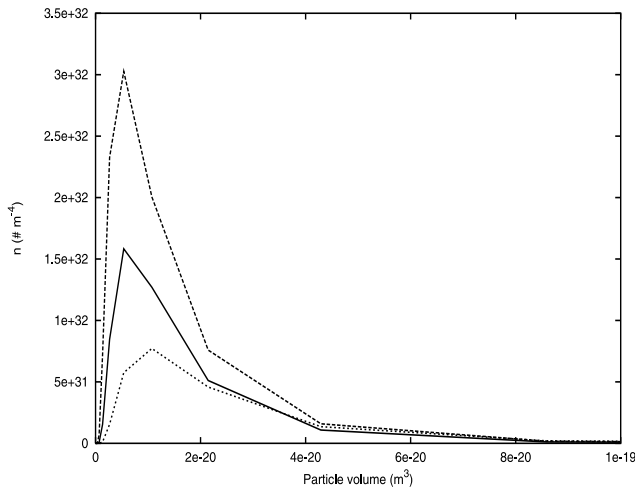


Fig. 1. Profiles of aerosol size distribution function at $t = 80$ s for three different simulation runs. Under nominal conditions (solid line), 20 ppm increase in the initial concentration of each reactant (long-dashed line), and 5 °C decrease in the initial fluid temperature (short-dashed line).

$$\frac{1 + Kn}{1 + 1.71Kn + 1.333Kn^2} dv$$

$$\frac{dC_1}{dt} = -k_r C_1 C_2$$

$$\frac{dC_2}{dt} = -k_r C_1 C_2$$

$$\frac{dT}{dt} = (k_r C_1 C_2 \Delta H_r + 4UD_T^{-1}(T_w - T))C_{pv}^{-1} \quad (38)$$

where ΔH_r is the heat of reaction, U is the overall heat transfer coefficient at the system boundary, T_w is the temperature at the system boundary of the heat transferring medium, and C_{pv} is the volumetric heat capacity of the fluid. For the purposes of simulation, the Fuchs–Sutugin expression for the Brownian coagulation coefficient (Eq. (7)) was used in the evaluation of the collision integrals $\beta_{x, y, z}$. Further, a geometric constraint was applied at the section boundaries ($v_i = 2v_i$, $i = 1, 2, \dots, m$; Gelbard et al., 1980; Landgrebe & Pratsinis, 1990). This allows simulating the size distribution over a wider particle volume spectrum and eliminates the need of using the discontinuous function θ in evaluating the collision integrals. The simplified expressions for the collision integrals are given below:

$${}^1\bar{\beta}_{i,j,l} = 0 \quad 1 \leq i, j < l-1, 2 \leq l \leq m$$

$${}^1\bar{\beta}_{i,l-1,l} = \int_{x_{i-1}}^{x_i} \int_{x_{l-1}-v}^{x_{l-1}} \frac{\beta(u, v)}{(x_i - x_{i-1})(x_{l-1} - x_{l-2})} dudv$$

$$1 \leq i < l-1, 2 \leq l \leq m$$

$${}^1\bar{\beta}_{l-1,l-1,l} = \int_{x_{l-2}}^{x_{l-1}} \int_{x_{l-2}}^{x_{l-1}} \frac{\beta(u, v)}{(x_{l-1} - x_{l-2})^2} dudv$$

$$2 \leq l \leq m$$

$${}^2\bar{\beta}_{i,l} = \int_{x_{i-1}}^{x_i} \int_{x_{l-v}}^{x_l} \frac{\beta(u, v)}{(x_i - x_{i-1})(x_l - x_{l-1})} dudv$$

$$i < l, 2 \leq l \leq m$$

$${}^3\bar{\beta}_{l,l} = \int_{x_{l-1}}^{x_l} \int_{x_{l-1}}^{x_l} \frac{\beta(u, v)}{(x_l - x_{l-1})^2} dudv \quad 1 \leq l \leq m$$

$${}^4\bar{\beta}_{i,l} = \int_{x_{i-1}}^{x_i} \int_{x_{l-1}}^{x_l} \frac{\beta(u, v)}{(x_i - x_{i-1})(x_l - x_{l-1})} dudv$$

$$l \leq i, 1 \leq l \leq m \quad (39)$$

The number of sections considered was 40 and the collision integrals in each section were evaluated using the Gauss Quadrature method. The process parameters used in the simulations are given in Table 2. Throughout the paper, the aerosol reactor is initially assumed to be filled with species A and B (the initial mole fractions of A and B are given in Table 2). We performed a set of simulation runs of the aerosol reactor to study the long-time behavior of the aerosol size distribution for three different sets of parameters. Fig. 1, displays the aerosol size distributions at the end of the three simulation runs ($t = 80$ s) for the nominal parameter values given in Table 2 (solid line), for the nominal parameter values and a 20 ppm increase in the initial concentration of each of the reactant species (long-dashed line), and for the nominal parameter values and a 5 °C decrease in the initial fluid temperature (short-dashed line). These results confirm a lognormal shape for the size distributions for long times and motivate the use of a unimodal lognormal moment model to obtain esti-

mates of the first three moments of the aerosol size distribution that describe key average properties of the aerosol product. In addition to the evolution of the entire size distribution, the sectional model can be used to obtain the total number concentration N_T , the geometric average particle volume v_g , and the geometric standard deviation σ from the following expressions (Landgrebe & Pratsinis, 1990):

$$N_T = \sum_{i=1}^m N_i \quad (40)$$

$$\ln v_g = \sum_{i=1}^m \frac{N_i}{N_T} \left(\frac{\Delta(v \ln v)_i}{\Delta v_i} - 1 \right) \quad (41)$$

$$\ln^2 \sigma_g = \frac{1}{9} \sum_{i=1}^m \frac{N_i}{N_T} \left(\frac{\Delta[v \ln^2(v/v_g)]_i - 2\Delta[v \ln v]_i + 2(1 + \ln v_g)}{\Delta v_i} \right) \quad (42)$$

where $\Delta(v \ln v)_i = v_i \ln v_i - v_{i-1} \ln v_{i-1}$ and $\Delta[v \ln^2(v/v_g)]_i = v_i \ln^2(v_i/v_g) - v_{i-1} \ln^2(v_{i-1}/v_g)$. The results for N_T , σ and v_g are presented later in this section.

Under the assumption of lognormal aerosol size distribution, the dimensionless model that describes the evolution of the first three moments of the distribution, along with the saturation ratio, reactant concentrations and fluid temperature, takes the form:

$$\frac{dN}{dt} = I' - \xi N^2$$

$$\frac{dV}{dt} = I'k^* + \eta(S - 1)N$$

$$\frac{dV_2}{dt} = I'k^{*2} + 2\varepsilon(S - 1)V + 2\zeta V^2$$

$$\frac{dS}{dt} = C\bar{C}_1\bar{C}_2 - I'k^* - \eta(S - 1)N$$

$$\frac{d\bar{C}_1}{dt} = -A_1\bar{C}_1\bar{C}_2$$

$$\frac{d\bar{C}_2}{dt} = -A_2\bar{C}_1\bar{C}_2$$

$$\frac{d\bar{T}}{dt} = B\bar{C}_1\bar{C}_2\bar{T} + E\bar{T}(\bar{T}_w - \bar{T}) \quad (43)$$

where \bar{C}_1 and \bar{C}_2 are the dimensionless reactant concentrations, \bar{T} , \bar{T}_w are the dimensionless fluid temperature and the dimensionless temperature of the heat transferring medium at the system boundary, respectively, and A_1 , A_2 , B , C , E are dimensionless quantities (the explicit expressions of A_1 , A_2 , B , C , E are given in Table 3).

We also performed a set of simulation runs to compare the predictions of the sectional and moment models for the conditions given in Tables 2 and 3, respectively. Fig. 2 shows the temporal evolution of the dimensionless total number concentration of the aerosol system, N , computed by the sectional (solid line) and moment (dashed line) models. As expected, N increases rapidly in the beginning due to a nucleation burst. However, there is an abrupt end to the increase in N once the nucleation subsides; thereafter N begins to decrease slowly as the new monomers being formed condense on the surface of particles and the particles coagulate to form bigger particles. Both coagulation and condensation cause the particles to grow in size, increasing the geometric average particle diameter, d_{pg} .

Table 3
Dimensionless variables for the model of Eq. (43)

$$A_1 = \tau k P_{o2} y_{2o} / RT_o$$

$$A_2 = \tau k P_{oy1o} / RT_o$$

$$B = P_o k \tau \Delta H_{\tau y1o y2o} / RT_o^2 C_p$$

$$C = N_{av} k \tau y_{1o} y_{2o} (P_o / RT_o)^2 / n_{so}$$

$$E = 4UR T_o \tau / D_T C_p P_o$$

$$\bar{C}_i = y_i / y_{io} \bar{T}$$

$$\bar{T} = T / T_o$$

$$\bar{T}_w = T_w / T_o$$

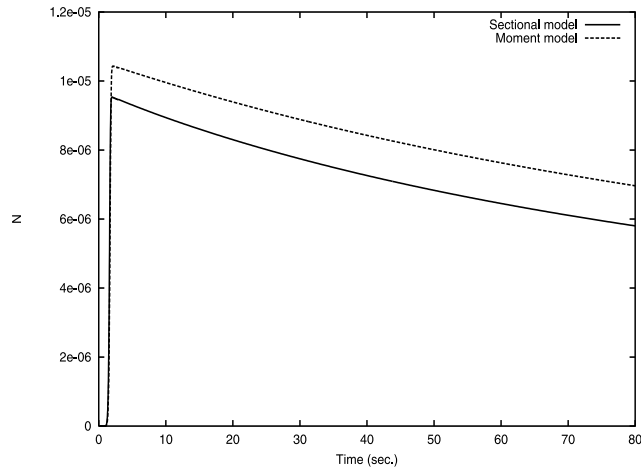


Fig. 2. Open-loop profiles of N computed by the sectional (solid line) and moment (dashed line) models.

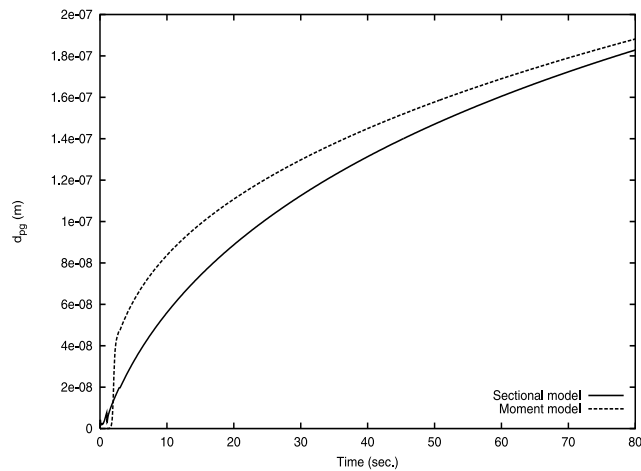


Fig. 3. Open-loop profiles of d_{pg} computed by the sectional (solid line) and moment (dashed line) models.

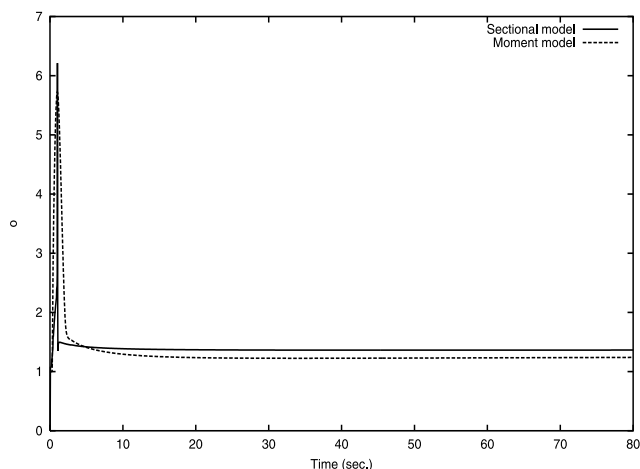


Fig. 4. Open-loop profiles of σ computed by the sectional (solid line) and moment (dashed line) models.

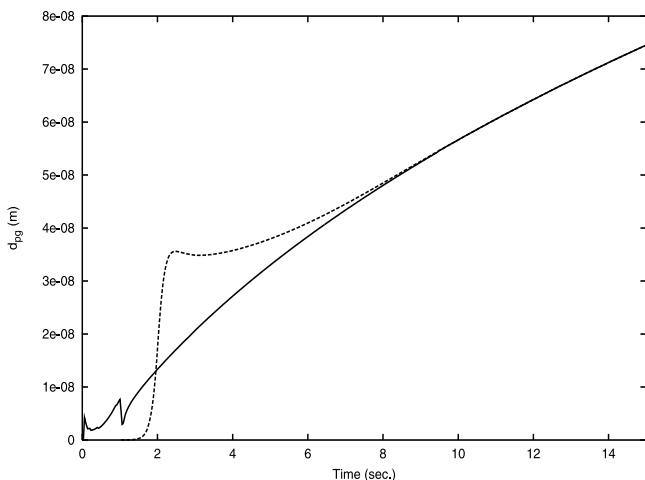


Fig. 5. Open-loop profiles of d_{pg} computed by the sectional model (solid line) and the moment model-based state estimator (dashed line) under nominal conditions.

This is evident from Fig. 3 which displays the profile of d_{pg} as a function of time, based on the sectional (solid line) and moment (dashed line) models. Fig. 4 presents the temporal evolution of the geometric standard deviation, σ , based on the sectional and moment models. Initially, the size distribution broadens as new particles nucleate and grow by Brownian coagulation and condensation. Eventually, nucleation subsides causing the low end of the particle size spectrum to deplete rapidly and the spread of the size distribution narrows resulting in an early maximum in σ . Thereafter, σ decreases to attain a final constant value of about 1.4 for the sectional model (solid line); this value is expected for an aerosol system with coagulation as the dominant growth phenomenon. Furthermore, in Fig. 4, we also observe that the moment model (dashed line) predicts a value for σ which is slightly lower than the value of σ predicted by the sectional model which is a consequence

of the assumption of unimodal lognormal size distribution made in the derivation of the moment model.

The results generated from the sectional and moment models show remarkable consistency. This justifies the use of lognormal moment models for the design of estimation and control systems for the aerosol process.

6. State estimation

A sectional model based observer design for an aerosol process may be unsuitable for use in systems that deliver real time responses. Motivated by the degree of consistency between the results of the sectional model and the lognormal moment model, we propose the use of the lognormal moment model for the design of a nonlinear estimator for the aerosol process which will yield estimates of average properties of the aerosol size distribution. This would result in an observer that can provide reasonable state estimates with minimal computational requirements, and is the subject of study in this section.

To begin our brief presentation on observer design, we first write the model of Eq. (43) in the following vector form:

$$\begin{aligned} \dot{\tilde{x}} &= \tilde{f}(\tilde{x}) + \tilde{g}(\tilde{x})u \\ y_i &= \tilde{h}_i(\tilde{x}), \quad i = 1, \dots, m \end{aligned} \tag{44}$$

where the explicit form of $\tilde{x}, \tilde{f}, \tilde{g}$ can be obtained by comparing Eqs. (43) and (44) and y_i denotes the i th measured output (e.g. geometric average particle diameter; see closed-loop simulations later in the section). An extended Luenberger-type observer has the following form (e.g. Chiu & Christofides, 1999):

$$\frac{d\omega}{dt} = \tilde{f}(\omega) + \tilde{g}(\omega)u + L(y - \tilde{h}(\omega)) \tag{45}$$

where ω denotes the observer state vector (the dimension of the vector ω is equal to the dimension of \tilde{x} in the system of Eq. (44)), $y = [y_1 \ y_2 \ \dots \ y_m]^T$ is the measured output vector, $\tilde{h}(\omega)$ is the estimated output vector and L is a matrix chosen so that the eigenvalues of the matrix $C_L = (\partial\tilde{f}/\partial\omega(\omega = \omega_s)) - L(\partial\tilde{h}/\partial\omega(\omega = \omega_s))$ where ω_s is the operating steady-state, $\partial\tilde{f}/\partial\omega$ and $\partial\tilde{h}/\partial\omega$ are Jacobian matrices of appropriate dimensions, lie in the open left-half of the complex plane. The state observer of Eq. (45) consists of a replica of the system of Eq. (44) plus a linear gain multiplying the discrepancy between the actual and the estimated values of the measured output.

We used the above methodology to construct a nonlinear state observer employing the moment model of Eq. (43) as the basis for design and using the geometric average particle diameter as the measured output. The observer gain was computed to guarantee that the state observer is an exponentially stable system. To study the ability of the nonlinear state observer to estimate aver-

age properties of the aerosol size distribution, we compare in Fig. 5 the estimated profile (dashed line) and the actual (solid line) profile (with the sectional model substituted for the actual process) of the geometric average particle diameter for the aerosol system under the conditions of Tables 2 and 3. It is clear that the observer estimates of d_{pg} converge very quickly to the true value computed by the sectional model; note that the results are shown from $t = 0$ to 15 s to show that the convergence of the estimation error is very fast compared to the entire batch cycle $t = 80$ s. Fig. 6 shows a similar plot but with errors in some of the modeling parameters (5% decrease in μ , 4% increase in D_f and 5% decrease in v_0). Again, the profile of the estimated value of d_{pg} (dashed line) converges to the value computed by the sectional model (solid line), thus showing the robustness of the observer in the presence of significant uncertainties

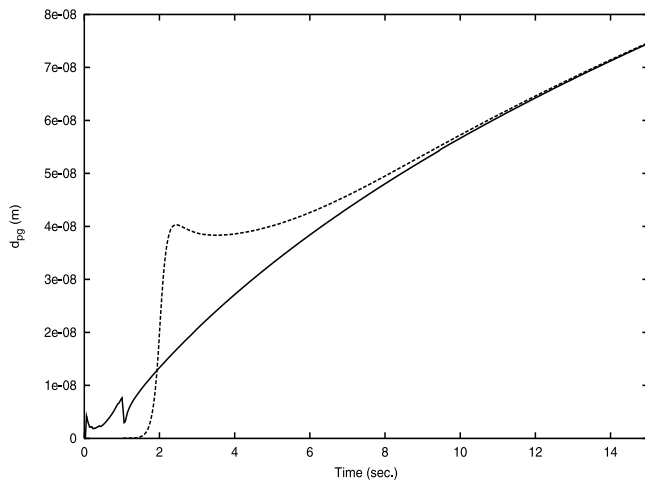


Fig. 6. Open-loop profiles of d_{pg} computed by the sectional model (solid line) and the moment model-based state estimator (dashed line) under parametric uncertainty in μ , D_f and v_0 .

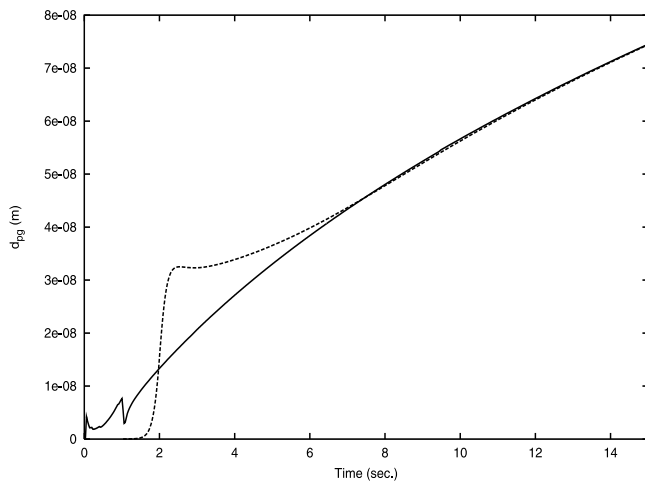


Fig. 7. Open-loop profiles of d_{pg} computed by the sectional model (solid line) and the moment model-based state estimator (dashed line) under parametric uncertainty in λ and γ .

in the model parameters. To further investigate the robustness of the state observer with respect to errors in model parameters, we show in Fig. 7 the profiles of the actual (solid line) and estimated (dashed line) values of d_{pg} in the presence of 7% increase in λ and 5% decrease in the surface tension value, γ . Again, the robustness properties of the state observer are excellent. Finally, it is important to note that it was verified that the state observer provides accurate estimates of the three leading moments of the aerosol size distribution, which is, of course, expected given the accuracy of the estimates of d_{pg} (detailed presentation of these results is omitted for brevity).

In the next section, the above state observer will be coupled with a nonlinear controller which will be designed on the basis of the moment model to lead to an output feedback controller that will be implemented on the sectional model to achieve tight control of d_{pg} .

7. Nonlinear control

We will begin with the design of the nonlinear controller, and we will follow with closed-loop simulations to study the robustness properties of the controller with respect to parametric model uncertainties and unmodeled actuator dynamics.

7.1. Output feedback controller synthesis

We use the model of Eq. (43) to synthesize a nonlinear finite-dimensional output feedback controller that guarantees stability and enforces output tracking in the closed-loop distributed parameter system. The output feedback controller is constructed through a standard combination of a state feedback controller with a state observer. The state feedback controller is synthesized via geometric control methods and the state observer is an extended Luenberger-type observer, as discussed in the previous section.

To proceed with our brief presentation of the controller synthesis results (more details can be found in Isidori, 1989 and are omitted here for brevity), we need to define the relative order of the output y_i with respect to the vector of manipulated inputs u as the smallest integer r_i for which

$$[L_{\tilde{g}_1} L_f^{r_i-1} \tilde{h}_1(\tilde{x}) \cdots L_{\tilde{g}_m} L_f^{r_i-1} \tilde{h}_m(\tilde{x})] \neq [0 \cdots 0] \quad (46)$$

where \tilde{g}_i is the i th vector of the matrix \tilde{g} , or $r_i = \infty$ if such an integer does not exist, and the characteristic matrix

$$C(\tilde{x}) = \begin{bmatrix} L_{\tilde{g}_1} L_f^{r_1-1} \tilde{h}_1(\tilde{x}) & \cdots & L_{\tilde{g}_m} L_f^{r_1-1} \tilde{h}_1(\tilde{x}) \\ L_{\tilde{g}_1} L_f^{r_2-1} \tilde{h}_2(\tilde{x}) & \cdots & L_{\tilde{g}_m} L_f^{r_2-1} \tilde{h}_2(\tilde{x}) \\ \vdots & \cdots & \vdots \\ L_{\tilde{g}_1} L_f^{r_m-1} \tilde{h}_m(\tilde{x}) & \cdots & L_{\tilde{g}_m} L_f^{r_m-1} \tilde{h}_m(\tilde{x}) \end{bmatrix} \quad (47)$$

The state feedback control problem is formulated as the one of synthesizing nonlinear state feedback controllers of the general form:

$$u = p(\tilde{x}) + Q(\tilde{x})v \quad (48)$$

where $p(\tilde{x})$ is a smooth vector function, $Q(\tilde{x})$ is a smooth matrix, and $v \in \mathcal{R}^m$ is the constant reference input vector, which guarantee local exponential stability and enforce a linear input–output response in the system of Eq. (44). This controller synthesis problem leads to the following nonlinear controller (Isidori, 1989):

$$u = \{[\beta_{1r_1} \cdots \beta_{mr_m}]C(\tilde{x})\}^{-1} \left\{ v - \sum_{i=1}^m \sum_{k=0}^{r_i} \beta_{ik} L_f^k \tilde{h}_i(\tilde{x}) \right\} \quad (49)$$

where the parameters β_{ik} are chosen so that the roots of the equation $\det(B(s)) = 0$ are in the open left-half of the complex plane ($B(s)$ is an $l \times l$ matrix, whose (i, j) th element is of the form $\sum_{k=0}^{r_i} \beta_{jk} s^k$). The controller of Eq. (49) enforces exponential stability in the closed-loop system, provided the unforced ($v \equiv 0$) zero dynamics of the system of Eq. (44) are locally exponentially stable.

The state feedback control law of Eq. (48) and the state observer of Eq. (45) can be combined to yield the following nonlinear output feedback controller:

$$\begin{aligned} \frac{d\omega}{dt} &= \tilde{f}(\omega) + L(y - \tilde{h}(\omega)) + \tilde{g}(\omega)[\beta_2 L_g L_f \tilde{h}(\omega)]^{-1} \{v - \beta_0 \tilde{h}(\omega) - \beta_1 L_f \tilde{h}(\omega) - \beta_2 L_f^2 \tilde{h}(\omega)\} \\ \tilde{u}(t) &= [\beta_2 L_g L_f \tilde{h}(\omega)]^{-1} \{v - \beta_0 \tilde{h}(\omega) - \beta_1 L_f \tilde{h}(\omega) - \beta_2 L_f^2 \tilde{h}(\omega)\} \end{aligned} \quad (52)$$

$$\begin{aligned} \frac{d\omega}{dt} &= \tilde{f}(\omega) + \tilde{g}(\omega) \{[\beta_{1r_1} \cdots \beta_{mr_m}]C(\omega)\}^{-1} \\ &\quad \times \left\{ v - \sum_{i=1}^m \sum_{k=0}^{r_i} \beta_{ik} L_f^k \tilde{h}_i(\omega) \right\} + L(y - \tilde{h}(\omega)) \\ u &= \{[\beta_{1r_1} \cdots \beta_{mr_m}]C(\omega)\}^{-1} \left\{ v - \sum_{i=1}^m \sum_{k=0}^{r_i} \beta_{ik} \tilde{h}_i(\omega) \right\} \end{aligned} \quad (50)$$

Remark 5: The exponential stability of the closed-loop system guarantees that in the presence of small initialization errors of the observer states (i.e. $\omega(0) \neq \tilde{x}(0)$), uncertainty in the process parameters and disturbances, the states of the closed-loop system will be bounded. Furthermore, it is possible to incorporate integral action in the nonlinear controller of Eq. (52) by substituting the term $v - \beta_0 \tilde{h}(\omega)$ (single-input single-output case) with the term $v - \beta_0 \tilde{h}(\tilde{x})$ (tracking error) to ensure asymptotic offsetless output tracking in the closed-loop system, in the presence of constant parametric uncertainty (see Daoutidis & Christofides, 1995 for details). Finally, the nonlinear controller of

Eq. (50) possesses a robustness property with respect to fast and asymptotically stable unmodeled dynamics (e.g. actuator and sensor dynamics, fast process dynamics; i.e. the controller enforces exponential stability and output tracking in the closed-loop system despite the presence of additional dynamics in the process, as long as they are stable and sufficiently fast).

7.2. Closed-loop simulations

We formulate the control problem as one of tracking the geometric average particle diameter of the aerosol system along a time-varying profile, by manipulating the wall temperature, i.e.:

$$y(t) = d_{pg}(t), \quad u(t) = \tilde{T}_w(t) - \tilde{T}_{ws} \quad (51)$$

where $\tilde{T}_{ws} = T_{ws}/T_0 = 1$. It was verified through open-loop simulations that the process model with the above manipulated input and controlled output is minimum phase. Therefore, the model of Eq. (44) was used as the basis for the synthesis of a nonlinear controller utilizing the control method described in the previous subsection. For this model, the relative order r was found to be equal to 2 and the necessary output feedback controller was synthesized using the formula of Eq. (50) and takes the form;

where v is the set-point, β_0 , β_1 , β_2 , and L are controller parameters and $\tilde{h}(\omega) = d_{pg}$. The tuning parameters of the controller were chosen as $\beta_0 = 1$, $\beta_1 = 25$ and $\beta_2 = 300$ to enforce a slightly underdamped response in the closed-loop system. The observer gain was chosen as in Section 6. Integral action was also incorporated in the nonlinear controller of Eq. (52) (i.e. the term $v - \beta_0 \tilde{h}(\omega)$ was substituted by $v - \beta_0 \tilde{h}(\tilde{x})$) to ensure offsetless tracking in the presence of constant uncertainty in process parameters. Since we are dealing with a batch operation, the reference input v is time-varying and is taken to be the desired profile for d_{pg} computed by the sectional model and shown in Fig. 3 (solid line). The practical implementation of the nonlinear controllers of Eq. (49) requires on-line measurements of d_{pg} ; in practice, such measurements can be obtained by using, for example, light scattering (see Rawlings et al., 1993 for details).

Several simulation runs were performed to evaluate the disturbance rejection and set-point tracking capabilities of the nonlinear controller, as well as its robustness with respect to uncertainty in model parameters and unmodeled actuator dynamics.

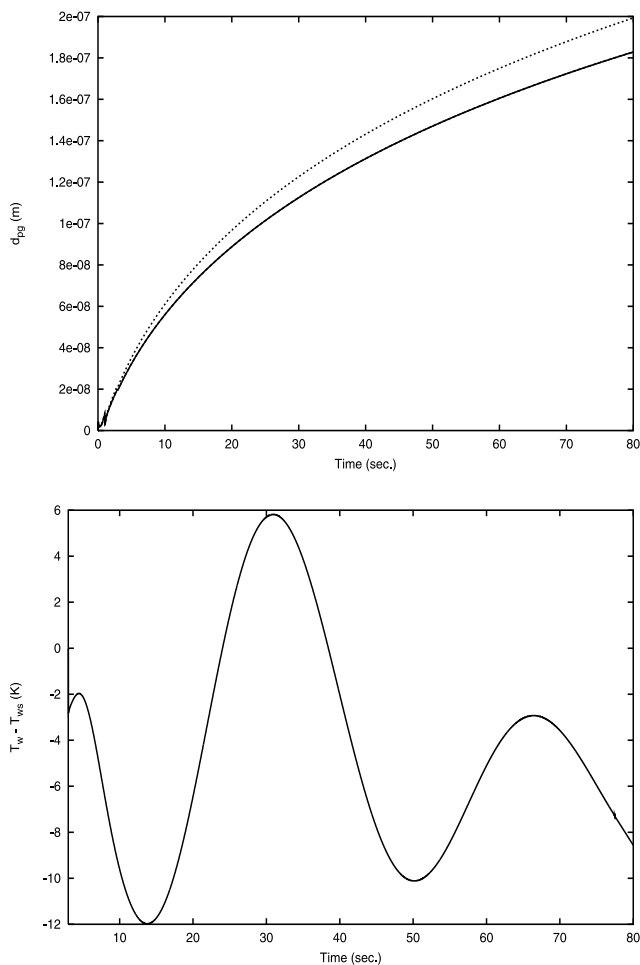


Fig. 8. Top plot, open-loop profile (dashed line) and closed-loop profile (solid line) of d_{pg} under uncertainty in the reaction rate constant. Bottom plot, manipulated input profile.

The first two simulation runs evaluate the performance of the nonlinear controller when there are significant errors in the modeling parameters. The objective of these simulations is to show that the use of feedback control allows producing an aerosol product with a desired geometric average particle diameter ($d_{pg} = 0.18 \mu\text{m}$ which is the value of d_{pg} for the open-loop system shown in Fig. 3 (solid line) computed with a constant wall temperature) within a given type of batch reactor and prespecified cycle time even in the case where the process model is not exactly known. Fig. 8 presents the open-loop profile (dashed line) and closed-loop profile (solid line) for d_{pg} (top plot), and the corresponding manipulated input profile (bottom plot) in the case of 6% error in the value of the rate constant, k . It is clear that the use of feedback control allows producing an aerosol product with a d_{pg} that exactly matches the desired one (i.e. $d_{pg} = 0.18 \mu\text{m}$) at the end of the batch cycle. Note that in the case of open-loop operation, the d_{pg} at the end of the batch cycle is about 10% off than the desired one, implying the need to

operate the process under feedback control. Fig. 9 presents the open-loop profile (dashed line) and closed-loop profile (solid line) for d_{pg} (top plot), and the corresponding manipulated input profile (bottom plot) in the case of a 8% decrease in the parameters used to evaluate the vapor pressure, P_s (refer to Table 2 for the nominal parameters). Again, the nonlinear controller allows achieving an aerosol product with the desired d_{pg} , clearly outperforming open-loop operation. Note that the manipulated input profiles in both runs are smooth functions of time.

We also tested the robustness properties of the nonlinear controller with respect to parametric model uncertainty and unmodeled actuator dynamics in the presence of a set-point change. Specifically, in addition to the parametric uncertainties considered in the previous two simulation runs, the process model of Eq. (38) was augmented with the following dynamical system, which represents the actuator dynamics, $\varepsilon_z z_1 = -z_1 + z_2$, $\varepsilon_z z_2 = -z_2 + u$, where $z_1, z_2 \in \mathcal{R}$ are the actuator states, z_1 is the actuator output

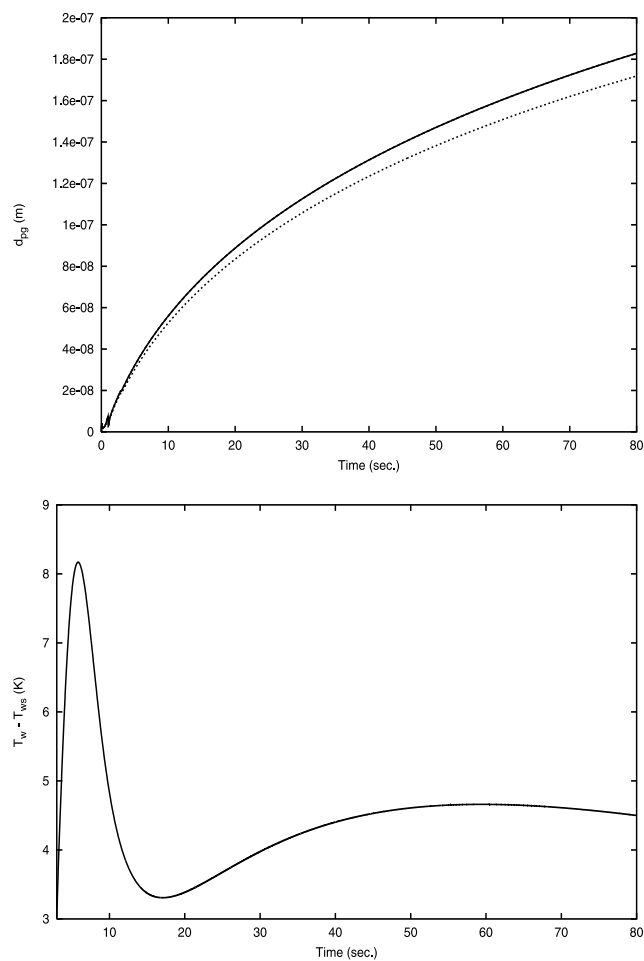


Fig. 9. Top plot, open-loop profile (dashed line) and closed-loop profile (solid line) of d_{pg} under uncertainty in the saturation pressure. Bottom plot, manipulated input profile.

and ϵ_z is a small parameter characterizing how fast are the actuator dynamics. For all values of $\epsilon < 1$, the nonlinear controller was found to exhibit very good robustness properties, keeping the output on the set-point profile (the profiles of d_{pg} for these simulation runs are very close to the closed-loop profiles of Figs. 8 and 9, and thus, they will be omitted for brevity).

Remark 6: It is important to point out that even though in our study we have chosen specific expressions for the nucleation, condensation and coagulation mechanisms in order to carry out the numerical calculations, the approach that we employed for the design of nonlinear estimators and controllers is applicable to most aerosol systems for which the hypothesis of unimodal lognormal aerosol size distribution for long times is valid. Finally, the interested reader may refer to Chiu and Christofides (1999), Kalani and Christofides (1999) for extensive comparisons of nonlinear control algorithms of the type used in the present simulation study with conventional proportional-integral control schemes that clearly demonstrate the superior performance and robustness properties of the nonlinear controllers.

8. Conclusions

In this work, we presented a comprehensive study on simulation, estimation and control of size distribution in aerosol processes with simultaneous chemical reaction, nucleation, condensation and coagulation. Initially, a typical aerosol process was considered and a detailed population balance model was presented which accounts for the aforementioned phenomena and describes how the aerosol size distribution evolves with time. The population balance was complemented with mass and energy balances that describe the evolution of the continuous phase species and temperature of the system. Sectional representations and lognormal moment approximations of the population balance model were then derived and used to simulate and provide estimates for the states of the process, respectively. It was found that a nonlinear state estimator based on the moment model provides accurate estimates of the average properties of the aerosol size distribution computed by the sectional model. The moment model, together with the species and energy balance equations were used as the basis for the synthesis of an output feedback controller which ensures that the geometric average particle diameter of the aerosol size distribution follows a prespecified trajectory. The robustness properties of the nonlinear estimator and controller with respect to significant parametric model uncertainty were successfully tested through computer simulations.

Acknowledgements

Financial support from a National Science Foundation CAREER award, CTS 9733509, and the Office of Naval Research (2001 Young Investigator Award) is gratefully acknowledged. The authors would also like to thank S.K. Friedlander for helpful suggestions.

Appendix A

The following aerosol growth phenomena were considered for the derivation of the integro-differential equations for the sectional model: (1) nucleation of aerosol particles, (2) growth by condensation of monomers on the aerosol particle surface, and (3) growth by coagulation. The mathematical derivation of the rate of change of the integral property, $Q_l(t)$ in section l , due to each of the above mentioned phenomenon is given below:

A.1. Nucleation

Nucleation of an aerosol particle with volume v^* in section l increases the property q by an amount, $\alpha v^{*\gamma}$. Given that the rate of nucleation in section l is: $I(v^*)\theta(v_{l-1} < v^* < v_l)$, the flux of Q_l into section l is given as:

$$\frac{dQ_l}{dt}\Big|_{\text{nucleation}} = \alpha v^{*\gamma} I(v^*) \theta(v_{l-1} < v^* < v_l) \quad (53)$$

A.2. Condensation

Diffusional condensation growth (the growth expression is given by Eq. (6)) may cause particles to exit the current section and enter the next higher section, as their size increases by condensation of monomers on the surface. Accounting for influx (due to condensation growth) of particles into section l from section $l-1$ and the outflux into section $l+1$, and substituting the variable ξ_l as defined in Section 3.1, the net flux of Q_l into section l is given as:

$$\begin{aligned} \frac{dQ_l}{dt}\Big|_{\text{condensation}} &= \alpha v_{l-1}^{\gamma/3} n(v_{l-1}, t) \xi_{l-1} \Delta v_l \\ &\quad - \alpha v_l^{\gamma/3} n(v_l, t) \xi_l \Delta v_l \end{aligned} \quad (54)$$

Substituting for $n(v, t)$ from Eq. (13), the above equation simplifies to the following:

$$\frac{dQ_l}{dt}\Big|_{\text{condensation}} = \xi_{l-1} Q_{l-1} - \xi_l Q_l \quad (55)$$

A.3. Coagulation

Coagulation may change the integral property Q_l in section l due to one of the following reasons (Gelbard

et al., 1980): (i) addition of particles to section l due to coagulation of particles in the lower sections, (ii) addition of particles to section l due to coagulation of particles in the lower sections with particles in section l , (iii) loss of particles from section/due to coagulation of particles in the lower sections with those in section l , (iv) loss of particles from section l due to coagulation of particles within section l , and (v) loss of particles from section l due to coagulation of particles in section l with particles in the higher sections.

The total rate of coagulation between particles in sections lower than l (note that $l > 1$) is given by:

$$\frac{1}{2} \int_{x_0}^{x_{l-1}} \int_{x_0}^{x_{l-1}} \beta(u, v)n(u, t)n(v, t)dudv \quad (56)$$

where u and v are the volumes of the colliding particles, x_0 is particle volume at the lower limit of the first section (i.e. the monomer volume) and x_{l-1} is the particle volume at the juncture of sections $l-1$ and l . The new particles being formed appear in section i only if their volume is greater than x_{l-1} and less than x_l . Thus, the net rate of addition of particles to section l is given by:

$$\frac{1}{2} \int_{x_0}^{x_{l-1}} \int_{x_0}^{x_{l-1}} \theta(x_{l-1} < u + v < x_l)\beta(u, v)n(u, t)n(v, t) \times dudv, \quad (57)$$

and hence, the flux of Q into section l due to coagulation of particles in the lower sections is given as:

$$\frac{1}{2} \int_{x_0}^{x_{l-1}} \int_{x_0}^{x_{l-1}} \alpha(u + v)^\gamma \theta(x_{l-1} < u + v < x_l)\beta(u, t)n(v, t) \times dudv \quad (58)$$

In order to account for the contributions of various sections to the change in Q_l , the integrals in Eq. (58) are replaced by a sum of integrals over each section as follows:

$$\frac{1}{2} \sum_{i=1}^{l-1} \sum_{j=1}^{l-1} \int_{x_{i-1}}^{x_i} \int_{x_{j-1}}^{x_j} \alpha(u + v)^\gamma \theta(x_{l-1} < u + v < x_l)\beta(u, v) \times n(u, t)n(v, t)dudv, \quad (59)$$

Substituting for n from Eq. (13), the following expression is obtained and represents the change in Q_i due to coagulation in the lower sections:

$$\frac{1}{2} \sum_{i=1}^{l-1} \sum_{j=1}^{l-1} Q_i Q_j \int_{x_{i-1}}^{x_i} \int_{x_{j-1}}^{x_j} \frac{(u + v)^\gamma \theta(x_{l-1} < u + v < x_l)\beta(u, v)}{\alpha u^\gamma v^\gamma (x_i - x_{i-1})(x_j - x_{j-1})} dvdu, \quad (60)$$

Following the derivation as described above, the flux of Q into section l due to coagulation of particles in section l with particles in lower sections is given by:

$$\int_{x_0}^{x_{l-1}} \int_{x_{l-1}}^{x_l} \alpha[(u + v)^\gamma - u^\gamma] \theta(u + v < x_l)\beta(u, v)n(u, t) \times n(v, t)dudv, \quad (61)$$

and the outflux of Q from section l due to coagulation of particles in lower sections with those in section l is given by:

$$\int_{x_0}^{x_{l-1}} \int_{x_{l-1}}^{x_l} \alpha u^\gamma \theta(u + v > x_l)\beta(u, v)n(u, t)n(v, t)dudv \quad (62)$$

Eqs. (61) and (62) may be added together and simplified to obtain the following:

$$Q_l \sum_{i=1}^{l-1} Q_i \int_{x_{i-1}}^{x_i} \int_{x_{i-1}}^{x_i} \frac{\{u^\gamma \theta(u + v > x_l) - [(u + v)^\gamma - u^\gamma]\}\beta(u, v)}{\alpha u^\gamma v^\gamma (x_i - x_{i-1})(x_i - x_{i-1})} dudv \quad (63)$$

Coagulation of particles within section l may result in a loss of Q_l either due to a reduction in the number of particles in section l or due to the formation of new particles with volume greater than x_l . The loss of Q_l due to the former phenomenon is given as:

$$\frac{1}{2} \int_{x_{l-1}}^{x_l} \int_{x_{l-1}}^{x_l} \alpha[u^\gamma + v^\gamma(u + v)^\gamma] \theta(u + v < x_l)\beta(u, v)n(u, t) \times n(v, t)dudv, \quad (64)$$

while the outflux of Q from section l due to the latter phenomenon is given by:

$$\frac{1}{2} \int_{x_{l-1}}^{x_l} \int_{x_{l-1}}^{x_l} \alpha(u^\gamma + v^\gamma) \theta(u + v > x_l)\beta(u, v)n(u, t)n(v, t) \times dudv \quad (65)$$

Adding together Eqs. (64) and (65) and simplifying, the following equation is obtained:

$$\frac{1}{2} Q_l^2 \int_{x_{l-1}}^{x_l} \int_{x_{l-1}}^{x_l} \frac{\{(u^\gamma + v^\gamma) \theta(u + v > x_l) + [u^\gamma + v^\gamma - (u + v)^\gamma]\}\beta(u, v)}{\alpha u^\gamma v^\gamma (x_l - x_{l-1})^2} dudv \quad (66)$$

Finally, the outflux of Q_l due to the coagulation of particles in section l with those in higher sections is given as (assuming m is the maximum number of sections being considered):

$$\int_{x_l}^{x_m} \int_{x_{l-1}}^{x_l} \alpha u^\gamma \beta(u, v)n(u, t)n(v, t)dudv, \quad (67)$$

which gives, on substitution of n from Eq. (13), the following expression:

$$Q_l \sum_{i=1}^m Q_i \int_{x_{i-1}}^{x_i} \int_{x_{l-1}}^{x_l} \frac{\{u^\gamma \beta(u, v)\}}{\alpha u^\gamma v^\gamma (x_i - x_{i-1})(x_l - x_{l-1})} dudv \quad (68)$$

The net rate of change of Q_l due to coagulation is obtained by adding the expressions in Eqs. (60), (63), (66) and (68):

$$\left. \frac{dQ_l}{dt} \right|_{\text{coagulation}} = \frac{1}{2} \sum_{i=1}^{l-1} \sum_{j=1}^{l-1} {}^1\bar{\beta}_{i,j,l} Q_i Q_j - Q_l \sum_{i=1}^{l-1} {}^2\bar{\beta}_{i,l} Q_i - \frac{1}{2} {}^3\bar{\beta}_{l,l} Q_l^2 - Q_l \sum_{i=1}^m {}^4\bar{\beta}_{i,l} Q_i, \quad (69)$$

where the collision integrals ${}^1\bar{\beta}_{i,j,l}$, ${}^2\bar{\beta}_{i,l}$, ${}^3\bar{\beta}_{l,l}$, ${}^4\bar{\beta}_{i,l}$, have the forms detailed in Eqs. (15)–(18).

Appendix B

In this Appendix, a derivation of the ODEs describing the evolution of the three leading moments of the aerosol in the free molecular size regime (Eqs. (22)–(24)), is given. The derivation of the moment equations in the continuum size regime (Eqs. (25)–(27)) is similar. The population balance equation (Eq. (1)) may be written as:

$$\begin{aligned} \frac{\partial n}{\partial t} = & -\frac{\partial(G_{\text{FM}}(\bar{x}, v)n)}{\partial v} + I(v^*)\delta(v - v^*) \\ & + \frac{1}{2} \int_0^v \beta_{\text{FM}}(v - \bar{v}, \bar{v})n(v - \bar{v})n(\bar{v})d\bar{v} \\ & - n(v) \int_0^\infty \beta_{\text{FM}}(v, \bar{v})n(\bar{v})d\bar{v} \end{aligned} \quad (70)$$

B.1. Zeroth moment

Integrating both sides of the equation from 0 to ∞ for the particle volume, making the substitution $v - \bar{v} = y$ in the third term on the right hand side and using that (Eq. (21)) $M_0 = \int_0^\infty n(v)dv$, we obtain:

$$\begin{aligned} \frac{dM_0}{dt} = & - \int_0^\infty \frac{\partial(G_{\text{FM}}(\bar{x}, v)n)}{\partial v} dv + I \\ & + \frac{1}{2} \int_0^\infty \int_0^\infty \beta_{\text{FM}}(y, \bar{v})n(y)n(\bar{v})d\bar{v}dy \\ & - \int_0^\infty \int_0^\infty \beta_{\text{FM}}(v, \bar{v})n(v)n(\bar{v})d\bar{v}dv \end{aligned} \quad (71)$$

The first term on the right hand side of Eq. (71) solves to zero. The collision frequency function β_{FM} , of Eq. (4) may be written as:

$$\beta_{\text{FM}}(v, \bar{v}) = B_1 b_0 (v^{-1/2} + \bar{v}^{-1/2})(v^{1/2} + \bar{v}^{1/2})^2 \quad (72)$$

Writing y as v , substituting the expression for β_{FM} and using Eq. (21) in Eq. (71), we get:

$$\begin{aligned} \frac{dM_0}{dt} = & I - \frac{B_1 b_0}{2} \int_0^\infty (M_0 v^{1/6} + 2M_{1/3} v^{-1/6} + M_{2/3} v^{-1/2} \\ & + M_{-1/2} v^{2/3} + 2M_{-1/6} v^{1/3} + M_{1/6} n(v)) dv \end{aligned} \quad (73)$$

Using Eq. (21) once again, we finally obtain Eq. (22):

$$\frac{dM_0}{dt} = I - B_1 b_0 (M_{2/3} M_{-1/2} + 2M_{1/3} M_{-1/6} + M_{1/6} M_0) \quad (74)$$

B.2. First moment

Multiplying both sides of Eq. (70) by v_1 , integrating

from 0 to ∞ for the particle volume, substituting the expression for G_{FM} from Eq. (4) and using that $M_1 = M_1 = \int_0^\infty vn(v)dv$, we obtain Eq. (23):

$$\frac{dM_1}{dt} = Iv^* + B_1(S - 1)M_{2/3} \quad (75)$$

B.3. Second moment:

Multiplying both sides of Eq. (70) by v^2 and performing calculations similar to the case for the zeroth moment (with coefficient b_2 used as b_0 in the expression of β_{FM}) we obtain Eq. (24):

$$\begin{aligned} \frac{dM_2}{dt} = & Iv^{*2} + 2B_1(S - 1)M_{5/3} \\ & + 2b_2 B_1 (M_{5/3} M_{1/2} + 2M_{4/3} M_{5/6} + M_{7/6} M_1) \end{aligned} \quad (76)$$

References

- Akhtar, M. K., Lipscomb, G. G., & Pratsinis, S. E. (1994). Monte carlo simulation of particle coagulation and sintering. *Aerosol Science and Technology*, 21, 83–93.
- Brock, J. R., Kuhn, P. J., & Zehavi, D. (1986). Condensation aerosol formation and growth in a laminar coaxial jet: experimental. *Journal of Aerosol Science*, 17, 11–22.
- Chiu, T., & Christofides, P. D. (1999). Nonlinear control of particulate processes. *American Institute of Chemical Engineers Journal*, 45, 1279–1297.
- Chiu, T., & Christofides, P. D. (2000). Robust control of particulate processes using uncertain population balances. *American Institute of Chemical Engineers Journal*, 46, 266–280.
- Daoutidis, P., & Christofides, P. D. (1995). Dynamic feedforward/output feedback control of nonlinear processes. *Chemical Engineering Science*, 50, 1889–2007.
- Dimitratos, J., Elicabe, G., & Georgakis, C. (1994). Control of emulsion polymerization reactors. *American Institute of Chemical Engineers Journal*, 40, 1993–2021.
- Eaton, J. W., & Rawlings, J. B. (1990). Feedback control of chemical processes using on-line optimization techniques. *Computers and Chemical Engineering*, 14, 469–479.
- El-Farra, N. H., Chiu, T. Y., & Christofides, P. D. (2001). Analysis and control of particulate processes with input constraints. *American Institute of Chemical Engineers Journal*, 47, 1849–1865.
- Frenklach, M., & Harris, S. J. (1987). Dynamic modeling using the method of moments. *Journal of Colloid Interface Science*, 118, 252–261.
- Friedlander, S. K. (1977). *Smoke, dust, and haze: fundamentals of aerosol behavior*. New York: Wiley.
- Friedlander, S. K. (1983). Dynamics of aerosol formation by chemical reaction. *Annals of New York Academy of Science*, 83, 354–364.
- Gelbard, F., Tambour, Y., & Seinfeld, J. H. (1980). Sectional representation of simulating aerosol dynamics. *Journal of Colloid Interface Science*, 68, 363–382.
- Gelbard, F., & Seinfeld, J. H. (1978). Numerical solution of the dynamic equation for particulate processes. *Journal of Computer Physics*, 28, 357–375.
- Hale, J. K., & Verduyn Lunel, S. M. (1993). *Introduction to functional differential equations*. New York: Springer.
- Hashemi, R., & Epstein, M. A. (1982). Observability and controllability considerations in crystallization process design. *American Institute of Chemical Engineers Symposium Series*, 78, 81–190.

- Hill, P. J., & Ng, K. M. (1995). New discretization procedure for the breakage equation. *American Institute of Chemical Engineers Journal*, 41, 1204–1216.
- Hill, P. J., & Ng, K. M. (1996). New discretization procedure for the agglomeration equation. *American Institute of Chemical Engineers Journal*, 42, 727–741.
- Hounslow, M. J. (1990). A discretized population balance for continuous systems at steady-state. *American Institute of Chemical Engineers Journal*, 36, 106–116.
- Isidori, A. (1989). *Nonlinear control systems: an introduction* (second ed.). Berlin, Heidelberg: Springer.
- Kalani, A., & Christofides, P. D. (1999). Nonlinear control of spatially-in homogeneous aerosol processes. *Chemical Engineering Science*, 54, 2669–2678.
- Kalani, A., & Christofides, P. D. (2000). Modeling and control of a titania aerosol reactor. *Aerosol Science and Technology*, 32, 369–391.
- Kumar, S., & Ramkrishna, D. (1996a). On the solution of population balance equations by discretization—I. A fixed pivot technique. *Chemical Engineering Science*, 51, 1311–1332.
- Kumar, S., & Ramkrishna, D. (1996b). On the solution of population balance equations by discretization—II. A moving pivot technique. *Chemical Engineering Science*, 51, 1333–1342.
- Landgrebe, J. D., & Pratsinis, S. E. (1990). A discrete sectional model for particulate production by gas phase chemical reaction and aerosol coagulation in the free molecular regime. *Journal of Colloid Interface Science*, 139, 63–86.
- Lee, K. W., Chen, H., & Gieseke, J. A. (1984). Log-normally preserving size distribution for Brownian coagulation in the free-molecule regime. *Aerosol Science and Technology*, 3, 53–62.
- Mantzaris, N. V., Daoutidis, P., & Sreenc, F. (2001). Numerical solution of multivariable cell population balance models. Parts: I, II and III. *Computers and Chemical Engineering*, 25, 1411–1481.
- Nicmanis, M., & Hounslow, M. J. (1998). Finite-element methods for steady-state population balance equations. *American Institute of Chemical Engineers Journal*, 44, 2258–2272.
- Pratsinis, S. E. (1988). Simultaneous nucleation, condensation, and coagulation in aerosol reactors. *Journal of Colloid Interface Science*, 124, 416–426.
- Ramkrishna, D. (1985). The status of population balances. *Review of Chemical Engineering*, 3, 49–95.
- Rawlings, J. B., & Ray, W. H. (1987). Emulsion polymerization reactor stability: simplified model analysis. *American Institute of Chemical Engineers Journal*, 33, 1663–1667.
- Rawlings, J. B., Miller, S. M., & Witkowski, W. R. (1993). Model identification and control of solution crystallization processes. *I&EC Research*, 32, 1275–1296.
- Rohani, S., & Bourne, J. R. (1990). Self-tuning control of crystal size distribution in a cooling batch crystallizer. *Chemical Engineering Science*, 12, 3457–3466.
- Semino, D., & Ray, W. H. (1995a). Control of systems described by population balance equations-I. Controllability analysis. *Chemical Engineering Science*, 50, 1805–1824.
- Semino, D., & Ray, W. H. (1995b). Control of systems described by population balance equations-II. Emulsion polymerization with constrained control action. *Chemical Engineering Science*, 50, 1825–1839.
- Tandon, P., & Rosner, D. E. (1999). Monte carlo simulation of particle aggregation and simultaneous restructuring. *Journal of Colloid Interface Science*, 213, 273–286.
- Van Peborgh Gooch, J. R., & Hounslow, M. J. (1996). Monte carlo simulation of size-enlargement mechanisms in crystallisation. *American Institute of Chemical Engineers Journal*, 42, 1864–1874.
- Williams, M. M. R., & Loyalka, S. K. (1991). *Aerosol science: theory and practice*. Oxford, UK: Pergamon Press.
- Xiong, Y., & Pratsinis, S. E. (1991). Gas phase production of particles in resctive turbulent flows. *Journal of Aerosol Science*, 12, 637–655.